Bioorganic Chemistry 93 (2019) 103311

Contents lists available at ScienceDirect

Bioorganic Chemistry

journal homepage: www.elsevier.com/locate/bioorg

The antiproliferative effect of spectinabilins from *Streptomyces spectabilis* on hepatocellular carcinoma cells *in vitro* and *in vivo*

Xiaoxiao Gao[a], Hongzhi Yao[a], Yu Mu[a], Peipei Guan[a], Guiding Li[b], Bin Lin[c], Yi Jiang[b,*], Li Han[a,*], Xueshi Huang[a,*], Chenglin Jiang[b]

[a] Institute of Microbial Pharmaceuticals, College of Life and Health Sciences, Northeastern University, Shenyang 110819, People's Republic of China
[b] Yunnan Institute of Microbiology, Yunnan University, Kunming 650091, People's Republic of China
[c] School of Pharmaceutical Engineering, Shenyang Pharmaceutical University, Shenyang 110016, People's Republic of China

ARTICLE INFO

Keywords:
Spectinabilin
2-Demethyl-spectinabilin
Hepatocellular carcinoma
SMMC7721
HepG2

ABSTRACT

Spectinabilin (**1**), spectinabilin derivative (**2**), and a new analogue, 2-demethyl-spectinabilin (**3**) were isolated from the fermentation broth of a soil-borne *Streptomyces spectabilis* strain. The structure of the new compound was elucidated by a detailed spectroscopic data analysis including data from CD spectra. Spectinabilin (**1**) demonstrated cytotoxicity against five human cancer cell lines, with IC_{50} values ranging from 18.7 ± 3.1 to 34.6 ± 4.7 μM, while derivatives **2** and **3** showed weak cytotoxicities. Notably, **1** inhibited the growth and proliferation of the hepatocellular carcinoma cell lines SMMC7721 and HepG2 in a time- and dose-dependent manner. Further study demonstrated that **1** caused G2/M phase cell cycle arrest in SMMC7721 and HepG2 cells through decreasing the protein levels of cyclin B1 and cdc2 as well as increasing that of p21. Compound **1** downregulated the protein expression of Bcl-2, upregulated Bax, and activated the cleavage of caspase-9 and -3 as a result of inducing apoptosis in SMMC7721 and HepG2 cells. Furthermore, the antitumor effect of **1** in SMMC7721 and HepG2 cells was mediated by the PI3K/AKT signaling pathway. In addition, **1** also suppressed tumor growth *in vivo* though inducing cell cycle arrest and apoptosis.

1. Introduction

Hepatocellular carcinoma (HCC), which is mainly associated with hepatitis B or C infection, cirrhosis, or nonalcoholic steatohepatitis, is one of the most prevalent types of primary liver malignancy [1,2]. It has become one of the leading causes of death worldwide [3]. Although the variety of effective therapeutic options has been improved, patients with advanced HCC or extrahepatic metastasis are unsuitable for surgical resection but are frequently considered candidates for chemotherapy [4,5]. However, the fact that HCC is highly resistant to conventional chemotherapeutic drugs results in unsatisfactory efficacy of chemotherapy [5]. Thus, the exploration of novel and effective antitumor molecules is required to prevent HCC development.

Spectinabilin (also named neoaureothin) and its homologoues are a group of pyrone metabolites produced by streptomycete [6]. Natural sources of spectinabilin homologoues are relatively rare, and only approximately twenty members were found up to this point, and all of them were produced by *Streptomyces* spp [6–12]. All of the compounds of this family consisted of a γ-pyrone or α-pyrone and a *p*-nitrobenzene moiety, and these two fragments were linked by a polyene chain. The length of the polyene chain of this group of compounds differed from diene (e.g. orinocin, luteoreticulin [13]) to sixene (e.g. homoneoaureothin [14]). Most of the homologoues were oxygenated at C-6 and formed a tetrahydrofuran ring between hydroxyl at C-6 and methyl at C-8 (e.g. aureothin, alloaureothin, spectinabilin, homoaureothin, and homoneoaureothin). Multiple biological activities of this family of metabolites were revealed: aureothin showed antimicrobial activity [15]; spectinabilin derivatives exhibited cytotoxicities [11–13]; SNF4435C and SNF4435D demonstrated immunosuppressive activity [16]; spectinabilin also inhibited RLV (Rauscher leukemia virus) reverse transcriptase and showed nematicidal activity [17,18].

In the process of our ongoing search for bioactive compounds from actinomycetes, the secondary metabolites of a soil-borne *Streptomyces spectabilis* (YIM 121038) were investigated based on the diverse chemical constituents illustrated through HPTLC and HPLC-MS analysis. Sixty liters of culture broth of *S. spectabilis* was extracted by EtOAc and fractionated, spectinabilin (**1**) [17], spectinabilin derivative (**2**) [11], and a new analogue, 2-demethyl-spectinabilin (**3**) were isolated by a series of chromatography methods (Fig. 1). The structures of 2-demethyl-spectinabilin (**3**) were elucidated by detailed spectroscopic data

* Corresponding authors.
E-mail addresses: jiangyi@ynu.edu.cn (Y. Jiang), hanli@mail.neu.edu.cn (L. Han), huangxs@mail.neu.edu.cn (X. Huang).

https://doi.org/10.1016/j.bioorg.2019.103311
Received 8 August 2019; Received in revised form 20 September 2019; Accepted 22 September 2019
Available online 24 September 2019

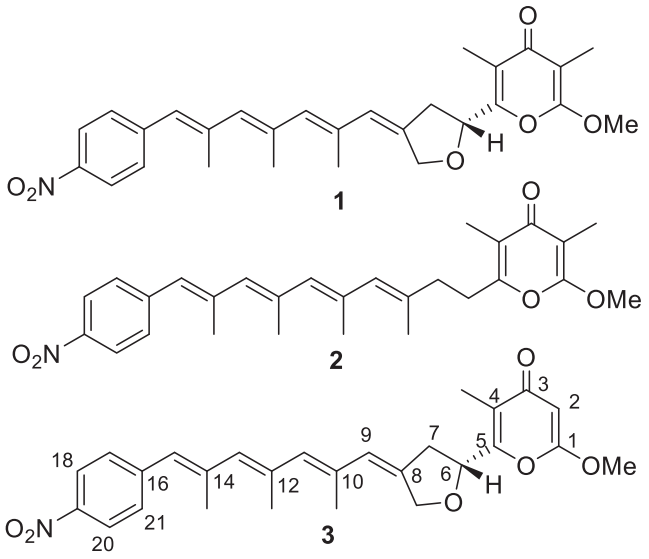

Fig. 1. Structures of 1–3.

analysis and CD spectra. The cytotoxicities of compounds **1–3** against five human cancer cell lines were evaluated and spectinabilin (**1**) showed better activities than compounds **2** and **3**, especially in HCC cells, SMMC7721 and HepG2 with IC_{50} values of 18.7 ± 3.1 and 23.9 ± 3.3 μM, respectively. In the present paper, we investigated the effect of spectinabilin on proliferation, apoptosis, and cell cycle arrest in two HCC cell lines, HepG2 and SMMC7721 *in vitro* and on growth inhibition in a xenograft model *in vivo*.

2. Experimental

2.1. General experimental procedures

Optical rotation was determined using an Anton Paar MCP200 automatic polarimeter (Graz, Austria). IR spectra were recorded with a Bruker Tensor 27 FT-IR spectrometer. ESI-MS were recorded on an Agilent 1290-6420 Triple Quadrupole LC-MS spectrometer (Santa Clara, CA, USA). HRESI-MS experiments were performed using a Bruker Micro TOF-Q mass spectrometer (Bruker Daltonics, Billerica, MA). NMR spectra were recorded on a Bruker Advance III-600 MHz and a Bruker AV-600 MHz spectrometer (Bruker, Rheinstetten, Germany). CD spectra were measured on a Biologic MOS-450 spectra polarimeter (Biologic Science, Claix, France). Silica gel (100–200 mesh, 200–300 mesh, Qingdao Marine Chemical, Ltd., Qingdao, China), Sephadex LH-20 (GE Healthcare Biosciences AB, Uppsala, Sweden), and YMC*GEL ODS-A (S-50 μm, 12 nm) (YMC Co., Ltd., Kyoto, Japan) were used for column chromatography. Flow cytometric analysis was conducted on an LSR-Fortessa flow cytometer (BD, Franklin Lakes, NJ, USA). MTT and protein quantification were analyzed by a microplate reader (BioTek Synergy H1, BioTek Instruments, Inc., Vermont, USA). The human breast adenocarcinoma cell line MCF-7, human melanoma cell line A375, human renal cell adenocarcinoma cell line 786-O, and human hepatocellular carcinoma cell lines SMMC7721 and HepG2 were purchased from the Chinese Academy of Science (Shanghai, China). Fetal bovine serum (FBS), penicillin, streptomycin, and L-glutamine were purchased from Gibco BRL Co., Ltd. (Gaithersburg, MD, USA). The primary antibodies for cyclin B1, cdc2, p21, Bax, Bcl-2, caspase-3, caspase-9, Akt, phospho-Akt (Ser473), PI3 kinase, phospho-PI3 kinase (Tyr458), GAPDH, and horse-radish peroxidase (HRP)-conjugated secondary antibodies were purchased from Cell Signaling Technology (Dancers, MA, USA).

2.2. Microbial material

The producing organism was isolated from a forest soil sample collected in Wuyi Mountains, Fujian Province, China. The strain was assigned to be *Streptomyces spectabilis* based on morphological characteristics and 16S rRNA gene sequences. The Blast result showed that the sequence was most similar (99.865%) to the sequence of *S. spectabilis* NBRC 13424 (GenBank accession no. AB184393). The strain (No. YIM 121038) was deposited in Yunnan Institute of Microbiology, Yunnan University, China.

2.3. Fermentation, extraction, and isolation

A slant culture of the strain was inoculated into 500 mL Erlenmeyer flasks each containing 100 mL of seed medium composed of 4 g L^{-1} yeast extract, 4 g L^{-1} glucose, 5 g L^{-1} malt extract, 3.75 mg L^{-1} multiple vitamins (thiamine 0.5 mg, riboflavin 0.5 mg, niacin 0.5 mg, pyridoxine 0.5 mg, inositol 0.5 mg, calcium pantothenate 0.5 mg, p-aminobenzoic acid 0.5 mg, biotin 0.25 mg), and 1 mL L^{-1} trace element solution (2 g L^{-1} $FeSO_4{\cdot}7H_2O$, 1 g L^{-1} $MnCl_2{\cdot}4H_2O$, 1 g L^{-1} $ZnSO_4{\cdot}7H_2O$). The pH was 7.2 with no adjustment, and the flasks were incubated for 2 days at 28 °C on a rotary shaker at 180 rpm. The seed culture was used to inoculate the fermentation broth with 10% volume. The large-scale fermentation was carried out in 1000 mL/2000 mL Erlenmeyer flasks with 200 mL/400 mL of fermentation media containing soybean meal 10 g L^{-1}, peptone 2 g L^{-1}, glucose 20 g L^{-1}, soluble starch 5 g L^{-1}, yeast extract 2 g L^{-1}, NaCl 4 g L^{-1}, K_2HPO_4 0.5 g L^{-1}, $MgSO_4{\cdot}7H_2O$ 0.5 g L^{-1}, $CaCO_3$ 2 g L^{-1}, with a pH of 7.8 with no adjustment, and the flasks were incubated for 7 days at 28 °C on a rotary shaker at 180 rpm.

The completed fermentation broth was clarified with a centrifuge to obtain 60 L of culture supernatant. Then, the supernatant was extracted with EtOAc four times. The combined EtOAc extracts were concentrated *in vacuo* to yield 23 g dried extract. The total extract was subjected to open silica gel (100–200 mesh) column chromatography with a CH_2Cl_2-MeOH solvent system (from 50:1 to 15:1, and 1:1 at last) to yield six fractions. Fraction 1 was subjected to Sephadex LH-20 chromatography (MeOH) to produce 6 subfractions (Fr.1.1-Fr.1.6). Fr.1.4 was further separated by silica gel (200–300 mesh) column chromatography (CH_2Cl_2-MeOH 50:1) to yield four subfractions (Fr.1.4.1-Fr.1.4.4). Then, Fr.1.4.4 was isolated by ODS column chromatography and eluted with MeOH-H_2O (60:40) to afford compound **2** (3.1 mg). Fr.1.5 was subjected to silica gel (200–300 mesh) column chromatography (CH_2Cl_2-MeOH 50:1) to yield compound **1** (148.0 mg). Compound **3** (5.8 mg) was obtained from Fr.1.6 by repeated silica gel column chromatography and eluted with CH_2Cl_2-MeOH (50:1).

2.4. 2-demethyl-spectinabilin (3)

Yellow oil; $[\alpha]_D^{20}$ = + 15.4 (*c* 0.52, MeOH); UV (MeOH) λ_{max} (log ε) 268 (3.82), 346 (3.77) nm; IR (film) ν_{max} 2925, 2854, 1660, 1624, 1592, 1514, 1448, 1411, 1377, 1338, 1248 cm^{-1}; CD (1.2 mg mL^{-1}, MeOH) λ_{max} ($\Delta\varepsilon$) 228 (14.10), 250 (−16.69) nm; ^1H and ^{13}C NMR see Table 1; ESIMS *m/z* 486 $[M+Na]^+$; HRESIMS *m/z*: 464.2047 $[M+H]^+$ (calcd for $C_{27}H_{30}NO_6$, 464.2073).

2.5. Cytotoxicity assay

The human breast adenocarcinoma cell line MCF-7, human melanoma cell line A375, and human hepatocellular carcinoma cell line HepG2 were cultured in DMEM medium. The human hepatocellular carcinoma cell line SMMC7721 and the human renal cell adenocarcinoma cell line 786-O were cultured in RPMI-1640 medium supplemented with 10% FBS, 1% L-glutamine, 100 units penicillin and 100 μg/mL streptomycin in a cell incubator (Thermo Fisher Scientific, Waltham, MA, USA) under standard culture conditions (37 °C, 5% CO_2

Table 1
^{1}H NMR (600 MHz) and ^{13}C NMR (150 MHz) Data for Compounds **2–3** in DMSO-d_6.

Position	**2**		**3**	
	δ_C, mult	δ_H, mult (*J* in Hz)	δ_C, mult	δ_H, mult (*J* in Hz)
1	162.3, C		167.4, C	
2	97.9, C		88.7, CH	5.59, s
3	179.8, C		180.3, C	
4	117.9, C		119.8, C	
5	158.4, C		157.2, C	
6	29.4, CH_2	2.78, t (7.0)	72.9, CH	5.12, t (7.0)
7	37.7, CH_2	2.38, t (7.0)	38.1, CH_2	2.99, dd (16.1, 7.0)2.82, dd (16.1, 7.0)
8	135.3, C		138.9, C	
9	131.2, CH	5.71, s	126.7, CH	6.09, s
10	134.4, C		134.7, C	
11	134.2, CH	5.78, s	135.4, CH	5.91, s
12	136.2, C		136.2, C	
13	134.4, CH	6.01, s	134.9, CH	6.05, s
14	140.0, C		139.9, C	
15	128.4, CH	6.57, s	128.6, CH	6.59, s
16	145.0, C		144.9, C	
17,21	130.3, CH	7.60, d (8.8)	130.3, CH	7.61, d (8.8)
18,20	124.0, CH	8.21, d (8.8)	124.0, CH	8.22, d (8.8)
19	145.7, C		145.8, C	
1-OCH_3	56.1, CH_3	3.97, s	57.0, CH_3	3.86, s
2-CH_3	7.4, CH_3	1.70, s		
4-CH_3	10.1, CH_3	1.83, s	9.1, CH_3	1.87, s
8-CH_3	18.2, CH_3	1.85, s		
8-CH_2O-			69.9, CH_2	4.78, d (14.0)4.62, d (14.0)
10-CH_3	19.6, CH_3	1.88, s	17.9, CH_3	1.97, s
12-CH_3	20.0, CH_3	2.02, s	20.0, CH_3	2.04, s
14-CH_3	19.8, CH_3	2.09, s	19.8, CH_3	2.10, s

humidified atmosphere). Cell viability was assessed by MTT assay. MCF-7, A375, 786-O, SMMC7721, and HepG2 cells were seeded in 96-well plates at a density of 7×10^3 cells/well and exposed to compounds **1–3** and adriamycin at six concentrations (0.33, 1.0, 3.3 10.0, 33.0 and 100 μM) for 48 h incubation. After that, 20 μL MTT was added to each well and incubated for another 4 h. Then, the media was removed and 150 μL DMSO was added to each well. A microreader was used to measure the absorbance at 570 nm. The inhibition rate (%) = [(A_{570}(control group)- A_{570}(experimental group)]/ A_{570}(control) × 100%. In addition, IC_{50} was calculated in GraphPad Prism 5.0 (GraphPad Software, Inc., CA, USA) with the nonlinear fit curve analysis with log-transformed concentrations. The results are represented as the mean ± SD from three independent experiments.

2.6. Measurement of cell cycle distribution

SMMC7721 and HepG2 cells were seeded in 6-well plates with a density of 5×10^5 cells/well and exposed to spectinabilin (0, 15.0 μM for SMMC7721; 0, 20.0 μM for HepG2, respectively) for 24 h. Cells were then collected and fixed overnight in 75% ethanol at −20 °C. The next day, the cells were washed twice with cold PBS and gently resuspended in 500 μL propidium iodide (PI) working fluid (Dingguo Changsheng Biotechnology Co. Ltd., Beijing, China) and then incubated for 15 min in the dark at room temperature. Cell cycle analysis was performed by using a LSR-Fortessa flow cytometer with a collection of 20,000 cells. The population of cells in each phase was analyzed using ModFit LT 4.1 software (Verity Software House, Topsham, Me, USA). Each experiment was conducted three times.

2.7. Measurement of apoptosis

SMMC7721 and HepG2 cells were seeded in 6-well plates with a density of 5×10^5 cells/well and exposed to spectinabilin (0, 15.0 μM for SMMC7721; 0, 20.0 μM for HepG2) for 24 h. Cells were then collected and washed with cold PBS and resuspended in 490 μL binding buffer and mixed with 5 μL of fluoresceine isothiocyanate (FITC)-conjugated annexin-V reagent and 5 μL PI (BD, Franklin Lakes, NJ, USA). After 15 min incubation at room temperature in the dark, samples were analyzed by flow cytometry with the Annexin V-FITC/PI apoptosis method. Cytographs were presented by BD FACSDiva Software (BD, Franklin Lakes, NJ, USA). Each experiment was conducted three times.

2.8. Western blot analysis

The *in vitro* effect of spectinabilin on protein expression was examined in SMMC7721 and HepG2 cells. SMMC7721 and HepG2 cells were seeded in 6-well plates with a density of 8×10^5 cells/well and treated with various concentrations (0, 1.67, 5.0 and 15.0 μM for SMMC7721; 0, 2.22, 6.67 and 20.0 μM for HepG2, respectively) of spectinabilin for 24 h. Treated cells were washed with cold PBS and lysed with RIPA lysis buffer (Beyotime Biotechnology Co., Shanghai, China) containing 2% protease inhibitor cocktail and 1% phosphatase inhibitor cocktail (Promega, Madison, WI, USA). The supernatant was collected and centrifuged at 15,000*g* for 15 min at 4 °C. In an *in vivo* experiment, tumor tissue homogenate was lysed for western blot. Protein concentration was determined by a BCA Protein Assay Kit (Beyotime Biotechnology Co., Shanghai, China). Equal quantities of protein (30–60 μg) were separated by 10% or 12% SDS-PAGE, electroblotted to polyvinylidene difluoride (PVDF) membranes (Millipore, Billerica, MA, USA), and blocked with 5% nonfat milk for 60 min at room temperature. The membranes were incubated with specific primary antibodies (diluted 1:3000 in 1 × TBS) overnight at 4 °C. After washing three times with TBST, the membranes were probed with corresponding secondary antibodies (diluted 1:10000 in 5% nonfat milk) for 60 min at room temperature. Then protein bands were detected with ECL select western blot detection reagent (Millipore, Billerica, MA, USA) by chemiluminescence (Tanon 5500, Shanghai, China). Each protein band was normalized to the respective anti-GAPDH band. The GIS Gel Image System (Tanon, Shanghai, China) was used for the quantitative grayscale analysis of the bands.

2.9. In vivo xenograft study

The experiments were performed in accordance with the Guide for the Care and Use of Laboratory Animals (Ministry of Science and Technology of China, 2006), and approved by the Laboratory Ethics Committees of College of Life and Health Science, Northeastern University (Shenyang, China). BALB/c nude mice (4-week-old, male) weighing approximately 18.0 ± 1.5 g were used to establish a xenograft model in the study. Mice were injected with 100 μL SMMC7721 suspension (5×10^6 cells) subcutaneously at the left flank. As the length diameter of the tumor reached approximately 3 mm, the mice were randomly allocated to three groups (n = 5). The treatment group was injected intraperitoneally with 100 μL spectinabilin (0.5 mg/kg and 1.0 mg/kg body weight, dissolved in 60% 1,2-propanediol) every other day for a total of 10 treatments. The control group was treated with vehicle in the same way. Body weight and tumor size were measured every other day. Tumor volume (mm^3) = length (mm) × width (mm) × depth (mm) × π/6. Then, the mice were sacrificed and the tumor were harvested for further study.

2.10. Data analysis

The results are presented as the mean ± standard deviation (SD) from at least three independent experiments. The differences of groups were analyzed using one-way analysis of variance with SPSS 13.0 (SPSS Inc., Chicago, IL, USA), followed by SNK (Student-Newman-Keuls) post hoc test. The threshold value for acceptance of difference was 5%

($p \leq 0.05$). The statistical analyses were performed using GraphPad Prism 5.0 (GraphPad Software, Inc., CA, USA).

3. Results and discussion

3.1. Isolation and structural elucidation

The large scale fermentation broth of *S. spectabilis* was clarified with a centrifuge to obtain 60 L of culture supernatant. The supernatant was extracted by EtOAc four times. The combined EtOAc extract (23 g) were isolated by sequential column chromatography over silica gel, Sephadex LH-20, and ODS to obtain pure compounds **1–3**. Compounds **1–2** were identified as spectinabilin (**1**) and spectinabilin derivative (**2**) by the ^{1}H NMR, ^{13}C NMR, and MS spectroscopic data analysis and comparison with the literature [11,17].

Compound **3** was isolated as a yellow oil, and the molecular formula was determined to be $C_{27}H_{29}NO_6$ by HRESIMS at *m/z* $[M+H]^+$ 464.2047 and ^{13}C NMR data. It showed 14 degrees of unsaturation. The ^{1}H NMR (Table 1) data of **3** indicated the presence of four aromatic protons as an AB system at δ_H = 8.22 (2H, d, J = 8.8 Hz) and δ_H = 7.61 (2H, d, J = 8.8 Hz), five singlet olefinic protons at δ_H = 6.59, 6.09, 6.05, 5.91 and 5.59, one oxygenated methine at δ_H = 5.12 (t, J = 7.0 Hz), one oxygenated methylene at δ_H = 4.78 (d, J = 14.0 Hz) and δ_H = 4.62 (d, J = 14.0 Hz), one methylene at δ_H = 2.99 (dd, J = 16.1, 7.0 Hz) and δ_H = 2.82 (dd, J = 16.1, 7.0 Hz), one methoxyl at δ_H = 3.86, and four singlet methyl groups at δ_H = 2.10, 2.04, 1.97 and 1.87. The ^{13}C NMR (Table 1) data displayed 27 carbon signals, 17 of which were unequivocally attributed to four aromatic methines, five olefinic methines, one oxygenated methine, two methylenes, one methoxyl, and four methyls on the basis of the HSQC experiment. In addition, one carbonyl and nine sp^2 carbons without directly bonded protons were observed from the ^{13}C NMR data. The ^{1}H and ^{13}C NMR data of **3** were closely related to the known compound spectinabilin (**1**) [17], which was also obtained from the same strain. Compared with **1**, **3** contained one highly shielded olefinic methine at δ_C = 88.7, δ_H = 5.59, and one nonbonded proton olefinic carbon and a methyl were absent. HMBC correlations (Fig. 2) observed from H-2 (δ_H = 5.59) to C-1 (δ_C = 167.4), C-3 (δ_C = 180.3), and C-4 (δ_C = 119.8) indicated that there was no substituent on C-2. The planar structure of **3**, as shown in Fig. 1, was further confirmed by ^{1}H–^{1}H COSY and HMBC correlations. The configuration of C-6 was determined as *R* according to the (-)-cotton effect at 250 nm indicated by CD spectra (Fig. 2), which were consistent with those of the congeners [14]. Thus, **3** was elucidated to be 2-demethyl spectinabilin.

Table 2
Cytotoxic (IC_{50} in μM) activities of compounds **1–3.**

Compound	1	2	3	Adriamycin
MCF-7	34.6 ± 4.7	> 100	> 100	3.8 ± 0.1
A375	29.7 ± 0.5	> 100	81.7 ± 1.6	0.5 ± 0.03
786-O	30.5 ± 1.0	49.7 ± 4.9	> 100	0.24 ± 0.04
HepG2	23.9 ± 3.3	> 100	66.8 ± 2.3	0.27 ± 0.01
SMMC7721	18.7 ± 3.1	57.4 ± 4.3	37.6 ± 3.7	0.31 ± 0.03

3.2. Cytotoxic activity

To evaluate the cytotoxic activity of compounds **1–3**, an MTT assay against a panel of human cancer cell lines were conducted. As shown in Table 2, spectinabilin (**1**) exhibited stronger cytotoxic activity against SMMC7721 and HepG2 cells among the five tested cancer cell lines, while compounds **2** and **3** exhibited weaker activity. The MTT assay results indicated that the five-membered furan ring in the spectinabilins' framework was quite favorable for the cytotoxic effects (**1**, **3** *vs.* **2**), and the methyl at C-2 significantly enhanced the cytotoxic activity (**1** *vs.* **3**). To evaluate the potential effect of **1** on the prevention of HCC development, further investigation of **1** against SMMC7721 and HepG2 cells were conducted. More profound anti-proliferative effects of **1** on SMMC7721 and HepG2 cells were observed in a time- and dose-dependent manner after spectinabilin treatment (Fig. 3), which demonstrated that **1** was an effective antitumor molecule to inhibit HCC cells. The proliferation rates also indicated that the viability of SMMC7721 and HepG2 cells was not significantly influenced by spectinabilin within 24 h at doses of 1.67–15.0 and 2.22–20.0 μM, respectively. Therefore, the effects of spectinabilin on apoptosis induction and cell cycle arrest in HCC cells were investigated at 24 h after drug treatment to avoid the interference caused by cell death.

3.3. Spectinabilin induced apoptosis in HCC cells

The dysregulation of cell apoptosis is closely correlated with the origination and progression of tumors [19]. Therefore, chemical agents that exert an effect on apoptosis induction may prove beneficial for tumor treatment [20]. To explore whether spectinabilin (**1**) induced apoptosis in HCC cells, apoptosis detection based on flow cytometric analysis was carried out. As shown in Fig. 4A, an increased population of apoptotic cells was identified in spectinabilin-treated SMMC7721 and HepG2 cells compared to the vehicle group. The results demonstrated that spectinabilin induced apoptosis in HCC cells. Apoptosis is mediated by a series of cellular events, and the alteration in the expression of key factors plays an important role in the apoptotic

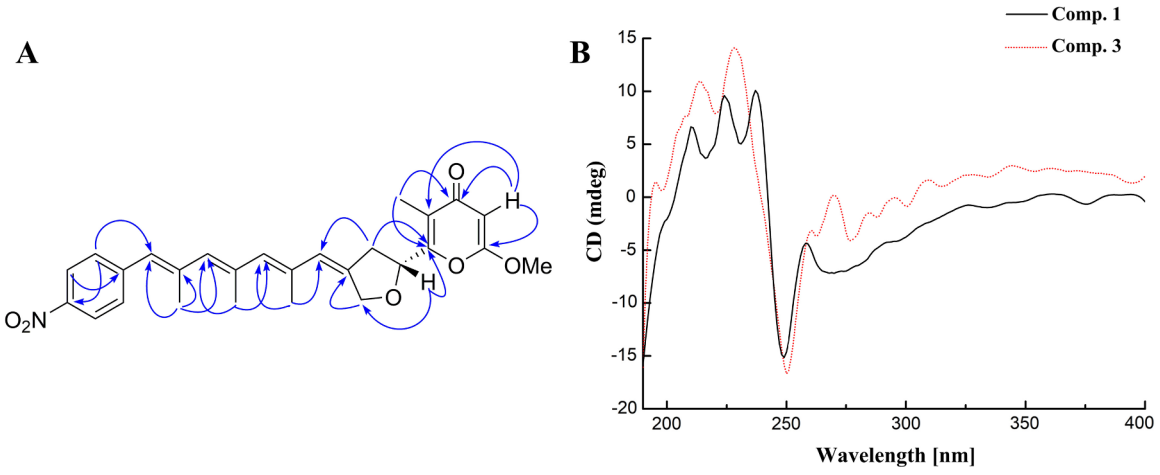

Fig. 2. Key HMBC correlations (A) and CD spectrum (B) of compound **3**.

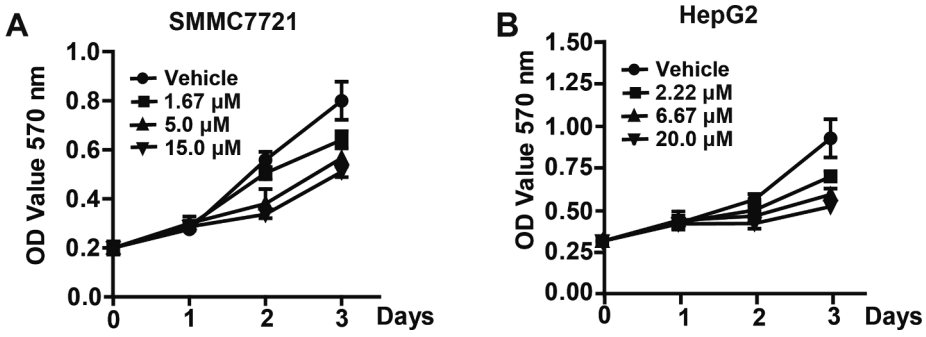

Fig. 3. Spectinabilin retarded the growth and proliferation of HCC cells. The growth curve of (A) SMMC7721 and (B) HepG2 cells treated with vehicle (con group) and various concentrations (1.67, 5.0 and 15.0 μM for SMMC7721 cells; 2.22, 6.67 and 20.0 μM for HepG2 cells) of spectinabilin for 3 days was detected by MTT assay.

signaling pathway. Bax and Bcl-2, which are well-characterized proteins in the Bcl-2 family, exert opposing effects on apoptosis [21,22]. The pro-apoptotic factor Bax is capable of making the outer membrane of mitochondria more porous to facilitate the release of some mitochondrial pro-apoptotic factors, while the anti-apoptotic factor Bcl-2 proves functions to prevent mitochondrial pore formation [23,24]. The enhancement of Bax over Bcl-2 triggers apoptosis-inducing factor release, which causes the activation of caspases [25]. Caspase-9 and caspase-3 play an important role in the progression of apoptosis. The inactive precursor of caspase-9 is usually activated by self-proteolysis and then triggers the activation of executioner caspase-3, resulting in the degradation of structural proteins, breakdown of DNA and finally induction of phagocytosis [26,27]. To investigate the underlying mechanism of spectinabilin on apoptosis induction, the expression of key

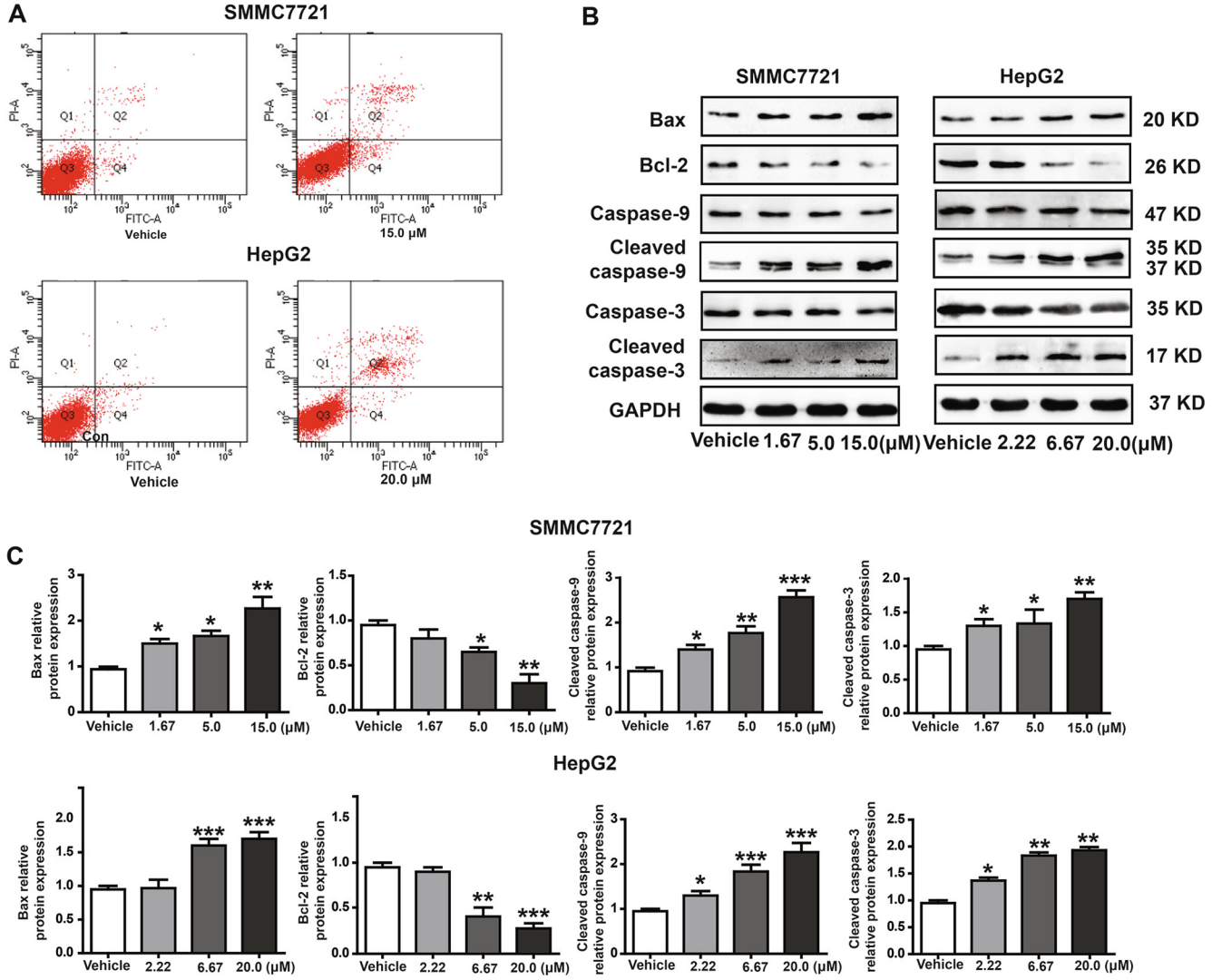

Fig. 4. Spectinabilin induced apoptosis in HCC cells. (A) Spectinabilin induced apoptosis was analyzed by flow cytometry in SMMC7721 and HepG2 cells treated with vehicle (con) and spectinabilin (15.0 μM for SMMC7721, and 20.0 μM for HepG2, respectively). (B) The protein levels of Bax, Bcl-2, caspase-9, cleaved caspase-9, caspase-3, and cleaved caspase-3 in SMMC7721 and HepG2 cells treated with vehicle (con) and various concentrations of spectinabilin (1.67, 5.0 and 15.0 μM for SMMC7721; 2.22, 6.67 and 20.0 μM for HepG2, respectively) were determined by western blot. (C) The relative quantities analysis of Bax, Bcl-2, cleaved caspase-9, and cleaved caspase-3 in SMMC7721 and HepG2 cells. $^{*}p < 0.05$, $^{**}p < 0.01$, and $^{***}p < 0.001$ *vs.* control.

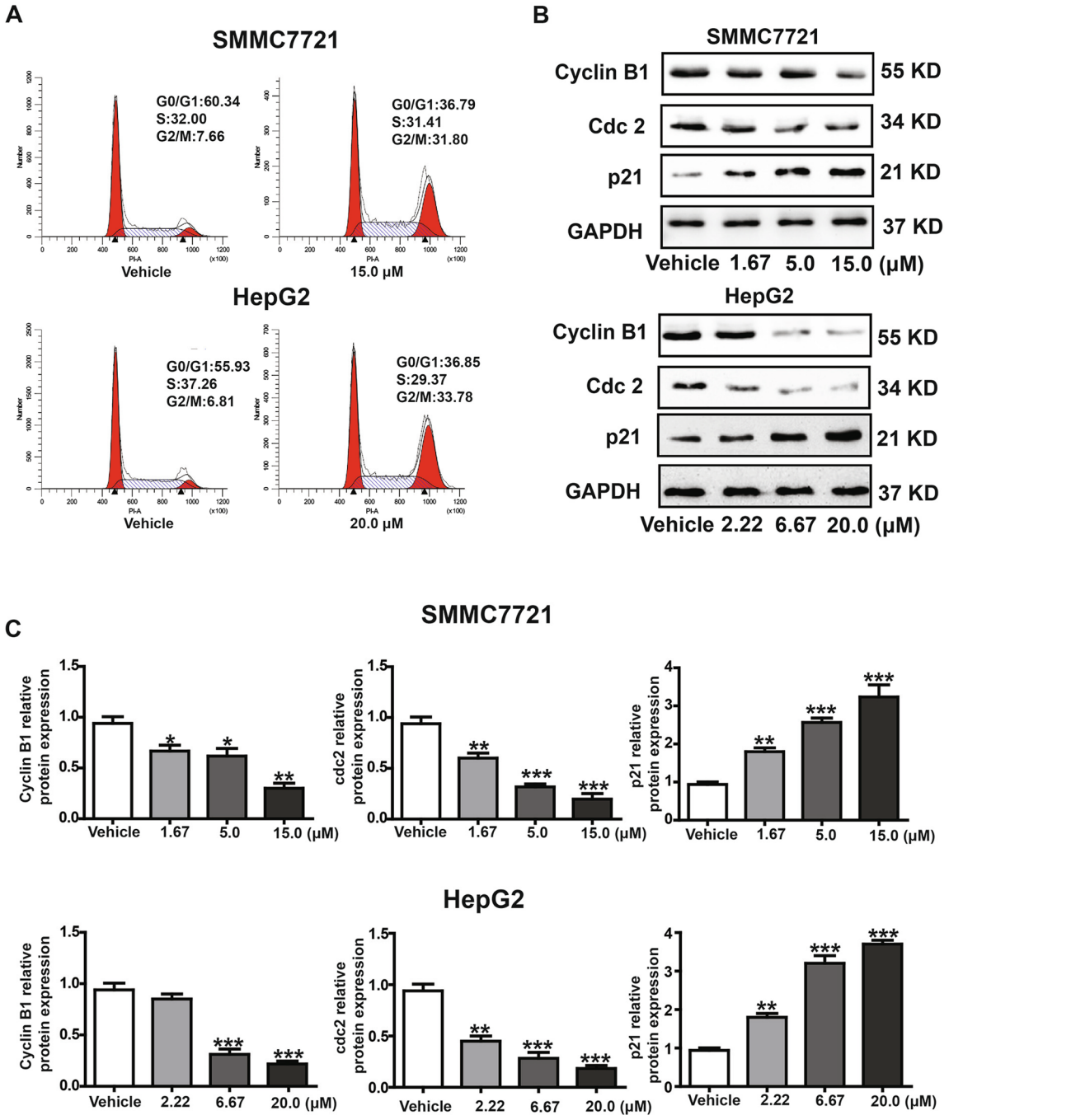

Fig. 5. Spectinabilin caused G2/M arrest in HCC cells. (A) Cell cycle distribution was analyzed by flow cytometry in SMMC7721 and HepG2 cells treated with vehicle (con) and spectinabilin (15.0 μM for SMMC7721, and 20.0 μM for HepG2, respectively). (B) The protein level of cyclin B1, cdc2 and p21 in SMMC7721 and HepG2 cells treated with vehicle (con) and various concentrations of spectinabilin (1.67, 5.0 and 15.0 μM for SMMC7721; 2.22, 6.67 and 20.0 μM for HepG2, respectively) was evaluated by western blot. (C) The relative quantities analysis of cyclin B1, cdc2, and p21 in SMMC7721 and HepG2 cells. *$p < 0.05$, **$p < 0.01$, and ***$p < 0.001$ *vs.* control.

factors associated with apoptosis was examined by western blot in spectinabilin-treated HCC cells. As shown in Fig. 4B and C, spectinabilin increased the protein levels of Bax, whereas decreased that of Bcl-2 in SMMC7721 and HepG2 cells in a dose-dependent manner. In addition, the expression levels of cleaved caspase-3 and caspase-9 were obviously increased compared to those of the vehicle group (Fig. 4B, C). Thus, spectinabilin induced apoptosis of SMMC7721 and HepG2 cells through upregulating the expression level of Bax, downregulating Bcl-2, and activating the caspase-dependent apoptotic signaling pathway.

3.4. Spectinabilin caused G2/M cell cycle arrest in HCC cells

The malfunction of the regulatory process of cell cycle progression results in uncontrolled cell proliferation in cancer cells [28]. Blocking cell cycle progression is considered another effective strategy to control tumor growth [29,30]. To determine the impact of spectinabilin (**1**) on cell cycle progression in HCC cells, cell cycle distribution in spectinabilin-treated SMMC7721 and HepG2 cells was analyzed by flow cytometry. As shown in Fig. 5A, the percentage of cells in G2/M phase

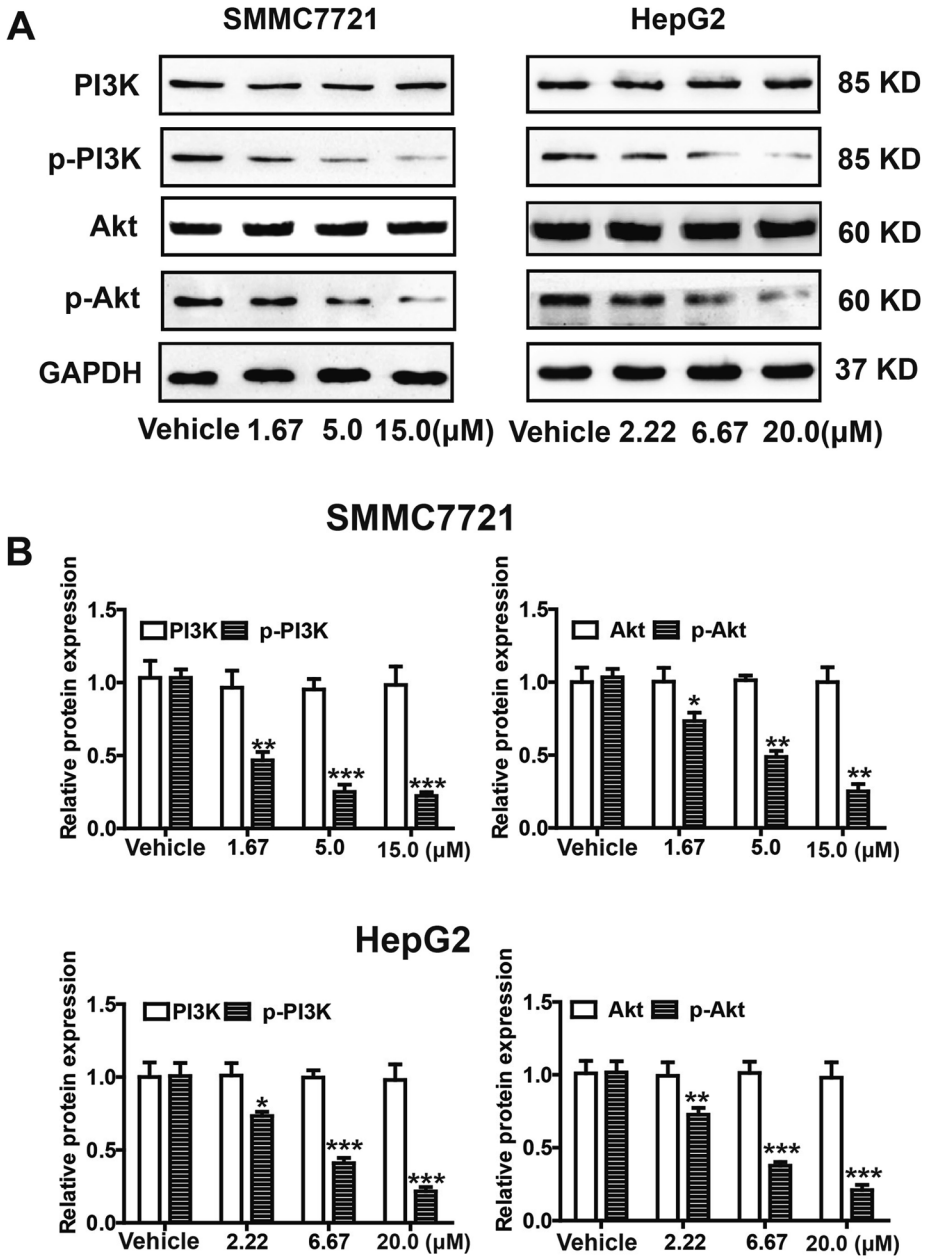

Fig. 6. Effect of spectinabilin on PI3K/AKT signaling pathway. (A) The protein expression of PI3K, p-PI3K, AKT and p-AKT was detected by western blot in SMMC7721 and HepG2 cells treated with vehicle (con) and various concentrations of spectinabilin (1.67, 5.0 and 15.0 μM for SMMC7721; 2.22, 6.67 and 20.0 μM for HepG2, respectively). (B) The relative quantities analysis of PI3K, p-PI3K, Akt, and p-Akt in SMMC7721 and HepG2 cells. $^{*}p < 0.05$, $^{**}p < 0.01$, and $^{***}p < 0.001$ *vs.* control.

increased obviously in spectinabilin-treated SMMC7721 and HepG2 cells. These results indicated that spectinabilin caused G2/M cell cycle arrest in HCC cells. Cell cycle progression is positively regulated by the active complex formed by cyclin-dependent kinases (CDKs) associated with specific cyclins [29]. In the G2/M phase, the cyclin B-cdc2 (CDK1) complex plays a pivotal role [31]. In addition, some cyclin-dependent kinase inhibitors (CKIs) show negative regulation of the cell cycle through binding to the subunits of CDKs [29,32]. p21, one of the most important CKIs, primarily binds with cdc2 to exhibit an inhibitory effect on the G2/M transition [33,34]. To further investigate the mechanism of spectinabilin in G2/M phase arrest, related regulators were examined by western blot in spectinabilin-treated SMMC7721 and HepG2 cells. As depicted in Fig. 5B and C, spectinabilin reduced the protein levels of cyclin B1 and cdc2, and increased that of p21 in a dose-dependent manner.

3.5. Spectinabilin downregulated PI3K/AKT signaling pathway in HCC cells

The PI3K/AKT signaling pathway is implicated in the regulation of a series of cellular events, such as proliferation, cellular transformation, tumorigenesis and tumor development [35]. Cumulative evidence has shown that aberrant activation of the PI3K/AKT pathway is commonly observed in HCC [35–38]. Thus, inhibition of this pathway is a promising method for HCC treatment. To investigate whether the antitumor effect of spectinabilin (**1**) in HCC cells was regulated by the PI3K/AKT signaling pathway, western blot analysis was performed. As shown in Fig. 6, treatment with spectinabilin significantly decreased the protein expression of phosphorylated PI3K and AKT in SMMC7721 and HepG2 cells in a dose-dependent manner. This result suggested that the antitumor effect induced by spectinabilin in HCC cells was related to the inhibition of the PI3K/AKT pathway.

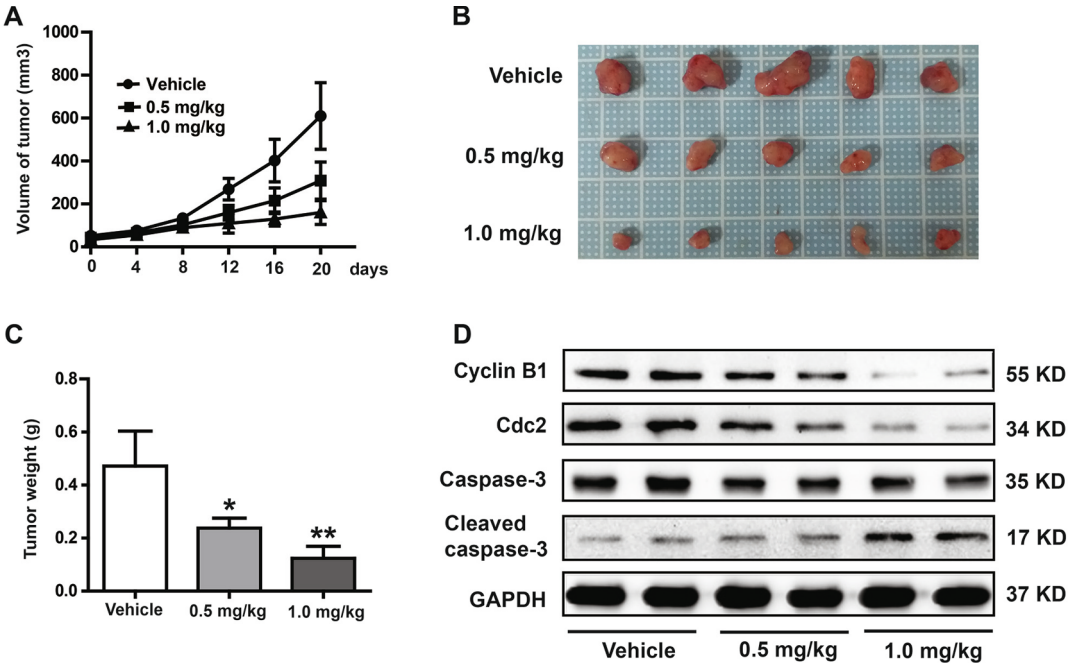

Fig. 7. Spectinabilin suppressed tumor growth *in vivo*. (A) Size of SMMC7721 tumor xenograft was measured at the indicated days. (B) Photograph of tumors removed from nude mice treated with vehicle (con) or spectinabilin (0.5 and 1.0 mg/kg body weight). (C) Tumor weight was scaled after mice sacrificed. (D) The protein level of cyclin B1, cdc2, caspse-3 and cleaved caspase-3 was determined by western blot. $*p < 0.05$, $**p < 0.01$ *vs.* control.

3.6. Spectinabilin suppressed SMMC7721 xenograft growth in vivo

The antitumor activity of spectinabilin (**1**) *in vivo* was investigated using a SMMC7721 xenograft mouse model. Compared to the control group, spectinabilin sharply reduced the tumor growth as the dose increased (Fig. 7A). At the end of the study, the average tumor volume and weight of the mice in the spectinabilin treatment group were considerably lower than those in the control group (Fig. 7B and C). The results confirmed the antitumor effect of spectinabilin *in vivo*. Furthermore, we conducted western blot analysis of tumor tissue homogenate to explore the underlying mechanism of the antitumor effect of spectinabilin *in vivo*. The results showed that the expression of cyclin B1 and cdc2 decreased, while cleaved caspase-3 increased after spectinabilin (0.5 mg/kg and 1.0 mg/kg) treatment. These results suggested that the antitumor mechanism of spectinabilin could also be derived from cell cycle arrest and apoptosis induction (Fig. 7D).

4. Conclusions

In summary, three spectinabilins (**1–3**) including a new compound 2-demethyl-spectinabilin (**3**) were isolated from a soil-borne *Streptomyces spectabilis*. Spectinabilin (**1**) inhibited the growth and proliferation of HCC SMMC7721 and HepG2 cell lines in a time- and dose-dependent manner. Spectinabilin caused G2/M phase arrest and induced apoptosis in SMMC7721 and HepG2 cells. The antitumor effect of spectinabilin in SMMC7721 and HepG2 cells was mediated by the PI3K/AKT signaling pathway. Spectinabilin suppressed tumor growth *in vivo* though inducing cell cycle arrest and apoptosis. All the results above strongly suggest that spectinabilin could be selected as an important lead molecule for the development of chemotherapy for HCC treatment. In depth investigation of the underlying mechanism of the antitumor effect and the *in vivo* safety of spectinabilin would be valuable in the future.

Declaration of Competing Interest

The authors declare no competing financial interest.

Acknowledgements

This work was funded by National Natural Science Foundation of China (Grant No. 81573327, 31460005) and the Fundamental Research Funds for the Central Universities, China (No. N172004004, N172006002, N172008008).

Appendix A. Supplementary material

Supplementary data to this article can be found online at https://doi.org/10.1016/j.bioorg.2019.103311.

References

[1] E.D. Ozer, N. Suna, A.S. Boyacioglu, Management of hepatocellular carcinoma: prevention, surveillance, diagnosis, and staging, Exp. Clin. Transplant. 15 (Suppl2) (2017) 31–35.
[2] T. Clark, S. Maximin, J. Meier, S. Pokhare, P. Bhargava, Hepatocellular carcinoma: review of epidemiology, screening, imaging diagnosis, response assessment, and treatment, Curr. Probl. Diagn. Radiol. 44 (2015) 479–486.
[3] R. Kumari, M.K. Sahu, A. Tripathy, K. Uthansingh, M. Behera, Hepatocellular carcinoma treatment: hurdles, advances and prospects, Hepatic Oncol. 5 (2) (2018) HEP08, https://doi.org/10.2217/hep-2018-0002.
[4] M. Ikeda, C. Morizane, M. Ueno, T. Okusaka, H. Ishii, J. Furuse, Chemotherapy for hepatocellular carcinoma: current status and future perspectives, Jpn. J. Clin. Oncol. 48 (2018) 103–114.
[5] J.-L. Raoul, J.-S. Frenel, J. Raimbourg, M. Gilabert, Current options and future possibilities for the systemic treatment of hepatocellular carcinoma, Hepatic Oncol. 6 (1) (2019) HEP11, https://doi.org/10.2217/hep-2019-0001.
[6] B. Busch, C. Hertweck, Evolution of metabolic diversity in polyketide-derived pyrones: using the non-colinear aureothin assembly line as a model system, Phytochemistry 70 (2009) 1833–1840.
[7] I. Yasuharu, N. Shigeru, S. Yoshikazu, Y. Shosuke, Total synthesis of (+)-iso-aureothm* determmatlon of the absolute configuratlons of aureothm, isoaureothm and spectinabilm, Tetrahedron Lett. 33 (1992) 521–524.
[8] T. Kawamura, T. Fujimaki, N. Hamanaka, K. Torii, H. Kobayashi, Y. Takahashi, M. Igarashi, N. Kinoshita, Y. Nishimura, E. Tashiro, M. Imoto, Isolation and structure elucidation of a novel androgen antagonist, arabilin, produced by Streptomyces sp. MK756-CF1, J. Antibiot. 63 (2010) 601–605.
[9] Y. Sugimoto, L. Ding, K. Ishida, C. Hertweck, Rational design of modular polyketide synthases: morphing the aureothin pathway into a luteoreticulin assembly line, Angew. Chem. Int. Ed. Engl. 53 (2014) 1560–1564.
[10] S.-H. Liu, M.-D. Xu, H. Zhang, H. Qi, J. Zhang, C.-X. Liu, J.-D. Wang, W.-S. Xiang, X.-J. Wang, New cytotoxic spectinabilin derivative from ant-associated Streptomyces

sp. 1H-GS5, J Antibiot 69 (2) (2016) 128–131, https://doi.org/10.1038/ja.2015.99.
[11] C.-X. Liu, S.-H. Liu, J.-W. Zhao, J. Zhang, X.-J. Wang, J.-S. Li, J.-D. Wang, W.-S. Xiang, A new spectinabilin derivative with cytotoxic activity from ant-derived Streptomyces sp. 1H-GS5, J. Asian Nat. Prod. Res. 19 (9) (2017) 924–929, https://doi.org/10.1080/10286020.2016.1254200.
[12] J.Y. Ueda, J. Hashimoto, A. Nagai, T. Nakashima, H. Komaki, K. Anzai, S. Harayama, T. Doi, T. Takahashi, K. Nagasawa, T. Natsume, M. Takagi, K. Shin-ya, New aureothin derivative, alloaureothin, from Streptomyces sp. MM23, J. Antibiot. 60 (2007) 321–324.
[13] M. Müller, B. Kusebauch, G. Liang, C.M. Beaudry, D. Trauner, C. Hertweck, Photochemical origin of the immunosuppressive SNF4435C/D and formation of orinocin through “polyene splicing”, Angew. Chem. Int. Ed. Engl. 45 (2006) 7835–7838.
[14] Y. Sugimoto, K. Ishida, N. Traitcheva, B. Busch, H.M. Dahse, C. Hertweck, Freedom and constraint in engineered noncolinear polyketide assembly lines, Chem. Biol. 22 (2015) 229–240.
[15] M. Taniguchi, M. Watanabe, K. Nagai, K. Suzumura, K. Suzuki, A. Tanaka, Gamma-pyrone compounds with selective and potent anti-helicobacter pylori activity, J. Antibiot. 53 (2000) 844–847.
[16] M.F. Jacobsen, J.E. Moses, R.M. Adlington, J.E. Baldwin, The total synthesis of spectinabilin and its biomimetic conversion to SNF4435C and SNF4435D, Org. Lett. 7 (2005) 2473–2476.
[17] K. Kakinuma, C.A. Hanson, K.L. Rinehart Jr., Spectinabilin, a new nitro-containing metabolite isolated from *streptomyces spectabilis*, Tetrahedron 32 (1976) 217–222.
[18] M.J. Liu, B.S. Hwang, C.Z. Jin, W.J. Li, D.J. Park, S.T. Seo, C.J. Kim, Screening, isolation and evaluation of a nematicidal compound from actinomycetes against the pine wood nematode, *bursaphelenchus xylophilus*, Pest. Manag. Sci. 75 (2019) 1585–1593.
[19] S. Elmore, Apoptosis: a review of programmed cell death, Toxicol. Pathol. 35 (2007) 495–516.
[20] G. Pistritto, D. Trisciuoglio, C. Ceci, A. Garufi, G. D'Orazi, Apoptosis as anticancer mechanism: function and dysfunction of its modulators and targeted therapeutic strategies, Aging 8 (2016) 603–619.
[21] M. Hassan, H. Watari, A. AbuAlmaaty, Y. Ohba, N. Sakuragi, Apoptosis and molecular targeting therapy in cancer, Biomed. Res. Int. 2014 (2014) 150845.
[22] J.M. Adams, S. Cory, The Bcl-2 protein family: arbiters of cell survival, Science 281 (1998) 1322–1326.
[23] S. Thomas, B.A. Quinn, S.K. Das, R. Dash, L. Emdad, S. Dasgupta, X.Y. Wang, P. Dent, J.C. Reed, M. Pellecchia, D. Sarkar, P.B. Fisher, Targeting the Bcl-2 family for cancer therapy, Exp. Opin. Ther. Targets 17 (2013) 61–75.
[24] A.M. Berghella, P. Pellegrini, I. Contasta, T. Del Beato, D. Adorno, Bcl-2 and drugs used in the treatment of cancer: new strategies of biotherapy which should not be underestimated, Cancer Biother. Radiopharm. 13 (1998) 225–237.
[25] F. Edlich, BCL-2 proteins and apoptosis: recent insights and unknowns, Biochem. Biophys. Res. Commun. 500 (2018) 26–34.
[26] A. Friedrich, J. Pechstein, C. Berens, A. Lührmann, Modulation of host cell apoptotic pathways by intracellular pathogens, Curr. Opin. Microbiol. 35 (2017) 88–99.
[27] A.G. Porter, R.U. Jänicke, Emerging roles of caspase-3 in apoptosis, Cell Death Differ. 6 (1999) 99–104.
[28] G.I. Evan, K.H. Vousden, Proliferation, cell cycle and apoptosis in cancer, Nature 411 (2001) 342–348.
[29] K. Vermeulen, D.R. Van Bockstaele, Z.N. Berneman, The cell cycle: a review of regulation, deregulation and therapeutic targets in cancer, Cell Prolif. 36 (2003) 131–149.
[30] S. Lapenna, A. Giordano, Cell cycle kinases as therapeutic targets for cancer, Nat. Rev. Drug Discov. 8 (2009) 547–566.
[31] X.H. Zhang, Z.Q. Zou, C.W. Xu, Y.Z. Shen, D. Li, Myricetin induces G2/M phase arrest in HepG2 cells by inhibiting the activity of the cyclin B/Cdc2 complex, Mol. Med. Rep. 4 (2011) 273–277.
[32] H. Gali-Muhtasib, N. Bakkar, Modulating cell cycle: current applications and prospects for future drug development, Curr. Cancer Drug Targets 2 (2002) 309–336.
[33] T. Ando, T. Kawabe, H. Ohara, B. Ducommun, M. Itoh, T. Okamoto, Involvement of the interaction between p21 and proliferating cell nuclear antigen for the maintenance of G2/M arrest after DNA damage, J. Biol. Chem. 276 (2001) 42971–42977.
[34] A.B. 3rd. Niculescu, X. Chen, M. Smeets, L. Hengst, C. Prives, S.I. Reed, Effects of p21(Cip1/Waf1) at both the G1/S and the G2/M cell cycle transitions: pRb is a critical determinant in blocking DNA replication and in preventing endoreduplication, Mol. Cell Biol. 18 (1998) 629–643.
[35] J. Liang, J.M. Slingerland, Multiple roles of the PI3K/PKB (Akt) pathway in cell cycle progression, Cell Cycle 2 (2003) 339–345.
[36] K. Blagotinsek, D. Rozman, Targeting signalling pathways in hepatocellular carcinoma, Curr. Pharm. Des. 23 (2017) 170–175.
[37] L. Ma, L. Ji, Y. Yu, J. Wang, Novel molecular targets for diagnosis and treatment of hepatocellular carcinoma, Discov. Med. 19 (2015) 7–14.
[38] Q. Zhou, V.W. Lui, W. Yeo, Targeting the PI3K/Akt/mTOR pathway in hepatocellular carcinoma, Future. Oncol. 7 (2011) 1149–1167.